Supporting Information

Direct Detection of Atmospheric Atomic Bromine Leading to Mercury and Ozone Depletion

Siyuan Wang, Stephen M. McNamara, Christopher W. Moore, Daniel Obrist, Alexandra Steffen, Angela R. W. Raso, Paul B. Shepson, Ralf M. Staebler, Kerri A. Pratt *

* Corresponding Author: Kerri A. Pratt

Department of Chemistry, University of Michigan, Ann Arbor
930 N. University Ave. Ann Arbor, Michigan 48109 USA
prattka@umich.edu
(734) 763-2871

Atomic Bromine Calibration Experiments

Flow Tube Setup and Br_2 Calibration. A quartz flow tube used for the calibration of atomic bromine in this work was adapted from previous chlorine monoxide (ClO) calibration experiments, as described by Custard et al (1). The flow tube is 122 cm long with an internal diameter of 6 cm. The inside of the flow tube, as well as glass connectors, were coated using Sylon CT (Sigma Aldrich) to occupy reactive surface sites to minimize wall losses. The flow tube is housed in a wooden box, surrounded by 6 light bulbs (PHILIPS 32W 3500K and SYLVANIA 32W 3500K) and a small fan to maintain room temperature. These light bulbs produce visible light in the range of ~400-700 nm. High purity N_2 boiling off from a liquid N_2 dewar was used as the carrier gas. A certified standard gas cylinder (Apel-Riemer Environmental) of 10.05 ppm (5% uncertainty) CH_3CHO in ultrapure N_2 was used in these experiments. Fluorinated ethylene propylene (FEP) tubing was utilized unless otherwise noted.

For each experiment, Br_2 was calibrated using a permeation source ($(80 \pm 3) \times 10^2$ ng min^{-1}, VICI), the rate of which was measured daily following the method of Liao et al (2). Br_2 mole ratios in the flow tube during experiments ranged from 3 to 22 ppb. Br_2 was

www.pnas.org/cgi/doi/10.1073/pnas.1900613116

monitored as $I^{79}Br^{79}Br^-$ at *m/z* 285 and $I^{79}Br^{81}Br^-$ at *m/z* 287 with dwell times of 500 ms each. Background signals were obtained when only N_2 was in the flow tube. Signals were background-subtracted and normalized to $I(H_2{}^{18}O)^-$ (*m/z* 147), yielding a normalized Br_2 sensitivity (*m/z* 287 / *m/z* 147 / [Br_2], Hz Hz^{-1} ppb^{-1}) of 1.86 ± 0.06 Hz Hz^{-1} ppb^{-1}. The ratio between m/z 285 and m/z 287 was 0.55 ± 0.02, consistent with the theoretical stable isotopic ratio of $^{79}Br_2$ vs $^{79}Br^{81}Br$ (0.51:1). Direct Br_2 injection (between 7 and 21 ppb) into the CIMS inlet without the flow tube yielded *m/z* 285 and 287 signals statistically indistinguishable from that determined with the flow tube, confirming the wall loss of Br_2 in flow tube was negligible.

Atomic Br Synthesis and Calibration. Atomic bromine was produced by the photolysis of gaseous Br_2, which absorbs strongly in the 350-600 nm wavelength range (3). The fluctuation of light intensity, which peaked between 410 and 550 nm, was <20% over 30 min (usually lights were turned on for <10 min). CH_3CHO was used to calculate the steady-state concentration of Br in the flow tube with lights on, because CH_3CHO does not absorb in the visible range (3) but reacts rapidly with atomic Br (4). Br_2 and CH_3CHO were injected into the flow tube, carried by 17 lpm of N_2. The residence time of the flow tube was 12 s. The total flow rate was chosen for a short residence time, but without creating turbulence (Reynolds number ~370), within the flow tube. The CIMS sampled 0.99 lpm from the centerline of the total flow, with the rest flowing to exhaust. Major species of interests monitored and corresponding dwell times during the flow tube experiments were: $IH_2{}^{18}O^-$ (*m/z* 147; 100 ms), $I^{79}Br^-$ and $I^{81}Br^-$ (*m/z* 206 and 208; 1000 ms each), $I^{79}Br^{79}Br^-$, $I^{79}Br^{81}Br^-$, and $I^{81}Br^{81}Br^-$ (*m/z* 285, 287, and 289; 500 ms each). Since *m/z* 208 signal could be from $I^{81}Br^-$ or $I(^{35}ClNO_2)^-$, $I(^{37}ClNO_2)^-$ at *m/z* 210 was also monitored with a dwell time of 1000 ms; *m/z* 210 ($ClNO_2$) was not observed in any of the flow tube experiment, confirming a lack of $ClNO_2$ contributing to *m/z* 208. The total duty cycle was 8 s in the first stage of the experiments and then was decreased to 6.2 s for later experiments after confirming the absence of certain species in the flow tube. The isotopic ratios were used to confirm the presence of Br in the flow tube experiments (Figure S3).

The general procedure for an experiment was as follows. CH_3CHO (33-203 ppb) was first injected at least 5 min prior to Br_2 injection to condition the CH_3CHO tubing and

the flow tube. Then Br_2 (1.9-7.0 ppb) was injected for 5-10 min while lights were off. Lights were then turned on for 5-10 min to commence the production of Br via Br_2 photolysis (and subsequent reaction with CH_3CHO). After this period, the lights were turned off, and both Br_2 and CH_3CHO flows were disconnected. Different levels of atomic bromine in the flow tube were obtained by varying Br_2 and CH_3CHO. Figure S3(a) shows an example of the time series of raw CIMS signals recorded during two representative experiments. Figure S3(b) shows the ratio between *m/z* 206 and 208 during all 15 experiments, when both Br_2 and CH_3CHO were injected with lights on. The ratio between *m/z* 206 and 208 was 1.113 ± 0.002, within 8% of the stable isotopic ratio of ^{79}Br / ^{81}Br (1.03), confirming the presence of Br as the dominant contributing species. Figure S4 shows CIMS mass scans under various experiment conditions. As shown, background signals of *m/z* 206 ($I^{79}Br^-$) and 208 ($I^{81}Br^-$) were both negligible (less than 8 Hz) without added Br_2 and with Br_2 in the dark, confirming the lack of Br atoms present prior to Br_2 photolysis. Therefore, the *m/z* 206 and 208 signals when Br_2 was injected in the dark were used as backgrounds for quantification of these signals during experiments. With the lights on, *m/z* 206 and 208 were both elevated (50-400 Hz, depending on Br_2 and CH_3CHO levels), confirming the presence of Br atoms upon turning on the lights and initiating Br_2 photolysis. The injection of CH_3CHO partially suppresses both *m/z* 206 and 208 due to the Br + CH_3CHO reaction.

Assuming steady-state for atomic bromine in the flow tube (meaning that Br produced from the photolysis of Br_2 is quenched by CH_3CHO), the steady-state Br concentration in the flow tube, $[Br]_{ss}$ (molec cm^{-3}), is calculated as:

$$[Br]_{ss} = \frac{2j_{Br_2}[Br_2]_{dark}}{k_{Br-CH_3CHO}[CH_3CHO]_{flowtube}} \quad \text{Eq.S1}$$

where j_{Br2} (s^{-1}) is the measured photolysis frequency of Br_2, $[Br_2]_{dark}$ (ppb) is the measured Br_2 mole ratio in the flow tube when the lights were off, $k_{Br\text{-}CH3CHO}$ (=(2.7±0.4) $\times 10^{-11}$ exp((-567±200)/T), (4)) is the literature rate coefficient of the reaction of Br + CH_3CHO (with kinetic uncertainties propagated into the total uncertainty) (4), and $[CH_3CHO]_{flowtube}$ (molec cm^{-3}) is the CH_3CHO concentration in the flow tube (calculated based on the

measured flow rate and dilution ratio, at the beginning of the flow tube with lights off). j_{Br2} was determined experimentally as follows:

$$j_{Br_2} = -\frac{\ln(\frac{[Br_2]_{light}}{[Br_2]_{dark}})}{\tau_{flowtube}} \quad \text{Eq.S2}$$

where $[Br_2]_{light}$ (ppb) is the measured Br_2 concentration in the flow tube when the lights were on, and $\tau_{flowtube}$ (s) is the flow tube residence time (12 s).

The calibration curve for Br is shown in Figure S3(c) as the background-subtracted and normalized *m/z* 206 ($I^{79}Br^-$) signal versus the Br steady-state concentration. The individual experimental Br sensitivities ranged from 2.3-3.0 Hz ppt^{-1}, with the Br sensitivity normalized to the reagent ion ($I(H_2{}^{18}O)^-$) at *m/z* 147 determined to be 0.00104 ± 0.00009 Hz Hz^{-1} ppt^{-1}. Uncertainties from the Br_2 permeation source (<8%), CH_3CHO standard (5%), kinetic uncertainty of CH_3CHO+Br reaction (~14%) (4), and all flow rate measurements were propagated into the total measurement uncertainty. The Br sensitivity factor relative to Br_2 was determined to be 0.56 ± 0.05 (with orthogonal distance regression fitting error, based on 15 experiments and associated uncertainties).

Investigating Potential Br Wall Loss, Br-Recombination, and Influence of NO_x and O_3 during Flow Tube Experiments. The wall loss rate of Br (k_{wall}, s^{-1}) in the flow tube can be estimated using a simple resistance model, based on Tang et al (5):

$$k_{wall} = \frac{\gamma_{eff}\bar{c}SA_{flowtube}}{4} \quad \text{Eq.S3}$$

where $\bar{c}$ (cm s^{-1}) is the mean molecular speed ($= 100\sqrt{\frac{8RT}{\pi MW}}$, with T as temperature, MW being the molecular weight of Br in kg mol^{-1}, and R as the ideal gas constant). $SA_{flowtube}$ (cm^2 cm^{-3}) is the inner-surface-area-to-volume-ratio of the flow tube (≈4/d, where d is the inner diameter of the flow tube, 6 cm). γ_{eff} (dimensionless) is the effective uptake coefficient of Br on the flow tube wall, which is determined by gas-diffusion and reactive uptake on the surface:

$$\frac{1}{\gamma_{eff}} = \frac{1}{\gamma} + \frac{\bar{c}d}{4\times 3.66\times D_g} \quad \text{Eq.S4}$$

where $\bar{c}$ is the mean Br molecular speed as above, γ (dimensionless) is the reactive uptake coefficient of Br on the flow tube wall, $\frac{\bar{c}d}{4\times3.66\times D_g}$ is the correction term for normalized gas-diffusion rate in a cylindrical tube, and D_g ($cm^2\ s^{-1}$) is the gas diffusivity. For rapid surface uptake, the overall process is limited by gas diffusion. At 298 K, assuming the maximum surface reactivity of Br on the flow tube wall ($\gamma = 1$), a typical gas diffusivity (0.1-0.2 $cm^2\ s^{-1}$) (5) leads to a Br wall loss characteristic time of 12-25 s. Note that the actual wall loss characteristic time is expected to be longer, since the inside of the flow tube was treated with Sylon CT. The minimum CH_3CHO concentration used in all experiments was 33 ppb, leading to the maximum calculated Br chemical lifetime of only 0.3 s, much shorter than the calculated Br wall loss characteristic time (12-25 s) and the flow tube residence time (12 s). Therefore, Br loss to the walls of the flow tube is expected to be negligible under the conditions of the Br calibration experiments.

In this study, the steady-state concentration of Br in the flow tube during experiments was <50 ppt. At 298 K, the Br re-combination rate to produce Br_2 (Br + Br + M → Br_2 + M; for M = N_2) is calculated to be $(8\pm3)\times10^{-33}\times[M]$ $cm^6\ molec^{-2}\ s^{-1}$ (6). Therefore, the characteristic time for Br re-combination for 50 ppt Br is calculated to be 4×10^3 s, much longer than that of Br+CH_3CHO reaction (< 0.3 s). Therefore, re-combination of Br in this work is not expected to be significant, and Br_2 reformed would subsequently photolyze.

Lastly, the possible influence of NO_x and O_3 in the calibration experiments can be ignored, as Br in the flow tube was primarily scavenged by CH_3CHO. NO in the flow tube was measured using a chemiluminescence detector (7) to be below the instrument LOD (70 ppt) during experiments. O_3 was measured to be below the instrument LOD (1 ppb) using an ozone monitor (Model 405, 2B Technologies). Using the kinetics summarized by Burkholder et al (3), the characteristic times of Br+NO_2 and Br+O_3 reactions were calculated as 118 s and 35 s, respectively, assuming the maximum possible levels (LODs: 70 ppt NO_2 and 1 ppb O_3) present in the flow tube. These are much longer than the characteristic time of the Br + CH_3CHO reaction (<0.3 s), such that Br was primarily lost through reaction with CH_3CHO, and it can be assumed that NO_2 and O_3 reactions with Br were negligible.

Br Production by $CHBr_3$ Photolysis. Additional experiments were performed to identify an alternate source of Br atoms via the photolysis of bromoform ($CHBr_3$). The photolysis of $CHBr_3$ was examined using the same flow tube as described in Section S2. $CHBr_3$ absorbs in the UV range (<300 nm), producing Br atoms (3). UV light bulbs (in the range of 300-420 nm, Q-Lab UVA340)(8) were used in this experiment. Figure S4(d) shows mass scans of flow tube background (N_2 only), ~17 ppm $CHBr_3$ under dark conditions, and $CHBr_3$ with UV lights on. Note that the dwell times of *m/z* 206 and 208 in the $CHBr_3$ mass scans were 200 ms. As shown, the signals for *m/z* 206 ($I^{79}Br^-$) and 208 ($I^{81}Br^-$) were negligible (<19 Hz) with only N_2 and for $CHBr_3$ added in the dark (<49 Hz). The presence of $CHBr_3$ was confirmed by the peaks detected at *m/z* 377 ($ICH^{79}Br_3^-$), 379 ($ICH^{79}Br^{81}Br_2^-$), 381 ($ICH^{79}Br_2^{81}Br^-$), and 383 ($ICH^{81}Br_3^-$), with relative peak intensities of 0.40:1.00:1.11:0.31, respectively, close to the theoretical isotope ratio of 0.34:1.00:0.98:0.32. When $CHBr_3$ added with lights on, *m/z* 206 ($I^{79}Br^-$) and 208 ($I^{81}Br^-$) were both elevated (up to 146 Hz), with the peak ratio (*m/z* 206 / *m/z* 208) being 1.0, consistent with the stable isotope ratio of ^{79}Br / ^{81}Br (1.03), confirming the production and detection of ~53 ppt Br from the photolysis of ~17 ppm $CHBr_3$.

Investigating Potential Fragmentation of Br-containing Species in CIMS. In this section, we show that the *m/z* 206 and 208 signals (IBr^-) detected in the field were not the result of fragmentation of Br_2, HOBr, or $CHBr_3$ from the chemical ionization process. Upon injection of up to 3.9 ppb of Br_2, ~two orders of magnitude higher than typically observed in the Arctic boundary layer (9–11), into the flow tube under dark conditions (no photolysis), signals at *m/z* 206 and 208 remained low (< 8 Hz). This confirms that Br_2 did not interfere with the measurement of Br at *m/z* 206 and 208 (Section S2.2, Figure S3 (a)). A similar argument can be made for HOBr as well. There is no evidence for a significant contribution to IBr^- from HOBr, due to the lack of correlation between the ambient Br (IBr^-) and HOBr ($IHOBr^-$) signals (Figure 1 and Figure 2). Similarly, $CHBr_3$ measured in the dark does not result in significant *m/z* 206 and 208 signals (Section S2.4 and Figure S4(d)). The ratio between *m/z* 206 and 208 in this study (background-subtracted) was always consistent with the stable isotope ratio of Br (Section S2.2), providing further evidence that the *m/z* 206 and 208 signals in this work can be uniquely attributed to atomic Br, rather than an artifact of the chemical ionization of other bromine species.

Unlike Br_2, HOBr, and $CHBr_3$, nitryl bromide ($BrNO_2$) can fragment and produce IBr^- signal at *m/z* 206 and 208 within the CIMS. To characterize this, $BrNO_2$ was synthesized by passing ~10 ppb Br_2 in N_2 over a solution of 0.1 M $NaNO_2$ (12), $BrNO_2$ was observed primarily as $IBrNO_2^-$ at *m/z* 252 and 254, with a *m/z* 252 / *m/z* 254 ratio of 1.06, consistent with the stable isotopic ratio of ^{79}Br and ^{81}Br (1.03). Signal at *m/z* 252 ($I^{79}BrNO_2^-$) was on average 6.5 ± 0.8 times greater than signal at *m/z* 206 ($I^{79}Br^-$). Similarly, *m/z* 254 ($I^{81}BrNO_2^-$) was 6.8 ± 0.9 times greater than signal at *m/z* 208 ($I^{81}Br^-$). We can apply these signal ratios to the 2012 BROMEX ambient measurements to estimate the maximum fraction of IBr^- signal that could be due to fragmentation of $BrNO_2$. For the BROMEX data, positive identification of $BrNO_2$ could not be achieved as the ratio of the signals at *m/z* 252 and *m/z* 254 were not in agreement with the corresponding natural isotopic abundance of ^{79}Br and ^{81}Br (1.03). Also, the *m/z* 254 signal did not rise above the background. At *m/z* 252, the signal was only above LOD and correlated with *m/z* 206 during two short periods (20:30 – 22:00 AKST 19 March 2012 and 7:30 – 9:30 AKST 20 March 2012). For context, the maximum normalized, background subtracted *m/z* 252 signal was 0.019 ± 0.005 Hz/Hz (8:39 – 9:14 AKDT 20 March 2012). Apply the ratio of 6.5 for $I^{79}BrNO_2^-/I^{79}Br^-$, we estimate that a maximum of 0.003 Hz/Hz of $I^{79}Br^-$ could potentially be attributed to $IBrNO_2^-$ fragmentation, which corresponds to 20% of the total observed signal of 0.015 Hz/Hz at *m/z* 206. This is within the average estimated uncertainty in Br during BROMEX of 23% + 0.2 ppt. However, to be cautious, for these two identified periods of potential interference, the IBr^- signal that was possibly due to $BrNO_2$ is accounted for in the errors bars of the Br atom mole ratios during this period, as shown in Figure 2.

Modeled Br / BrO ratios: Importance of Br_2

Here, we examine uncertainties in the modeled Br/BrO ratio and show that Br_2 has a significant impact on Br/BrO ratios during ODEs. For comparison to measurements, Br/BrO ratios were modeled by constraining to measured Br_2, BrO, ClO, temperature, TUV-calculated j-values (10). NO_x was varied from 10 to 193 ppt based on previous measurements during March 2009 near Utqiaġvik, AK (13). The modeled Br/BrO ratio is

very sensitive to NO_x and O_3, as shown in Figure S6. The modeled Br/BrO ratios track the measured values, but are overestimated by up to a factor of 3 when O_3 was below ~2 ppb, and underestimated by up to a factor of 5 when O_3 was above ~2 ppb. When O_3 was below ~2 ppb, the model uncertainty in the Br/BrO ratio was dominated by the O_3 measurement uncertainty; in contrast, when O_3 was above ~2 ppb, the model uncertainty in the Br/BrO ratio was dominated by the estimated range in NO_x. With respect to both model uncertainties and CIMS measurement uncertainties, the modeled Br/BrO ratio was in agreement with the modeled Br/BrO ratio calculated based on CIMS measurements. This analysis highlights the importance of NO_x measurements, as well as high accuracy O_3 measurements at sub-ppb levels.

Table S1 summarizes the calculated Br / BrO ratio for two previous field campaigns (Alert 2000: 29 April – 6 May 2000 in Alert, Canada; and OASIS 2009: 26-29 March 2009 in Utqiaġvik, AK) in which O_3 was both completely depleted (<2 ppb). In the case of OASIS 2009, mean Br_2 observed during the entire ODE was 2.5 ppt (11); We calculate the Br / BrO ratio to be underestimated by up to a factor of 4.3 if Br_2 is not considered (calculated Br / BrO: 19.3 and 4.4 with and without observed Br_2, respectively, Table S1). During OASIS 2009, BrCl was also measured (14); Figure S7 shows that, when O_3 was above ~20 ppb, the BrCl contribution to Br production is expected to be as important as that of Br_2. Therefore, under these conditions, the bias in modeled Br/BrO is expected to be even larger than when considering only Br_2. Considering available data from Alert 2000 (Table S1), the Br/BrO ratio is estimated to be 1.0 at 1.7 ppb O_3. However, Br_2 was not measured during Alert 2000. If we consider the presence of only 1 ppt Br_2, the calculated Br/BrO ratio would be enhanced by 50%, again showing the importance of knowledge of molecular halogen levels for the calculation of Br/BrO ratios and Br atom mole ratios.

Br-induced O_3 loss: a case study

During BROMEX, a complete O_3 depletion event was observed on 15 March 2012 (Figure 1), and the observed O_3 loss rate was up to 3 ppb h^{-1}. The Br measurements enabled the direct calculation of Br-induced ozone loss. Br-induced O_3 loss can be calculated using Equation S5 and measured Br, O_3, and BrO (Section S4) (15):

$$O_3\ Loss\ by\ Br = k_{Br+O_3}[Br][O_3] - j_{BrO}[BrO] - k_{BrO+NO}[BrO][NO] \quad \text{Eq.S5}$$

Here, O_3 is lost via reaction with Br (R2) and regenerated via BrO photolysis (R3) and reaction with NO (R4) (16). Figure S8 shows the observed O_3 loss rate, as well as the direct calculation using Br measurements (Eq.1). Due to the lack of NO_x measurements, an observationally constrained box-model was used to calculate NO_x (10). As previously described by Wang and Pratt, the model was constrained to measured Br_2 and NO_x was tuned until modeled BrO and HOBr were both in reasonable agreement with CIMS observations (mostly within ~35%, consistent with the measurement uncertainties of BrO and HOBr). The modeled NO_x mole ratio (10) in the case of 15 March 2012 was 69±28 ppt (average±standard deviation) (10), in reasonable agreement with spring 2009 NO_x measurements at Utqiaġvik, AK (up to 193 ppt) (11, 13). The calculated bromine-induced O_3 loss rate (Figure S8) is in good agreement with observations, implying the O_3 loss on 15 March was dominated by local reactive bromine chemistry. We have therefore demonstrated that with the Br measurements, the O_3 chemical loss rate can be directly calculated using Eq.1, which is the definition of O_3 chemical loss.

Apparent rate coefficient of bromine-induced Hg^0 oxidation

Br-induced Hg^0 oxidation occurs via reaction to produce HgBr (R.S1) (17). HgBr (i.e. Hg^I) is unstable and can undergo thermal decomposition to produce Hg^0 (R.S2), or react with Br or NO_2 to reproduce Hg^0 (R.S3 and R.S4) (17). HgBr can also be further oxidized into Hg^{II}, such as $HgBr_2$ or $HgBrNO_2$, respectively (via R.S5 or R.S6).

$$Hg^0 + Br + M \rightarrow HgBr + M \quad \text{R.S1}$$

$$HgBr + M \rightarrow Hg^0 + Br \quad \text{R.S2}$$

$$HgBr + Br \rightarrow Hg^0 + Br_2 \quad \text{R.S3}$$

$$HgBr + Br \rightarrow HgBr^2 \quad \text{R.S4}$$

$$HgBr + NO_2 \rightarrow Hg^0 + BrNO_2 \quad \text{R.S5}$$

$$HgBr + NO_2 \rightarrow HgBrNO_2 \quad \text{R.S6}$$

The dependence of Hg oxidation on Br and NO_2 is shown in Figures S9. Our calculation suggests more rapid Hg^0 loss at colder temperatures and higher Br mole ratios. With less than ~10 ppt NO_2, the apparent Hg^0 loss rate scales with NO_2 mixing ratios, but above ~10 ppt NO_2, the Hg^0 loss rate becomes less sensitive to the NO_2 levels.

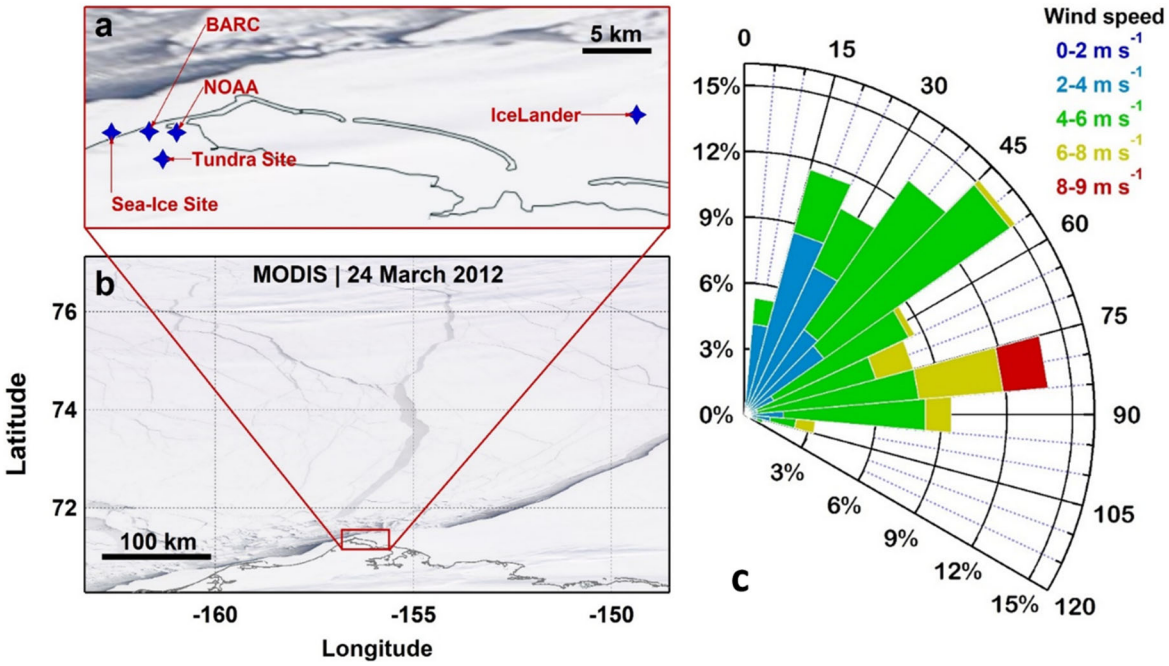

Figure S1. Measurement site locations during the BROMEX study (18) **and corresponding sea ice and snow conditions on 24 March 2012 (a and b), as well as the wind direction and speed from 14-28 March 2012 (c).** The satellite image (30 m and 125 m resolution in panels (a) and (b), respectively; NASA Moderate Resolution Imaging Spectroradiometer (MODIS): https://modis.gsfc.nasa.gov/) represents sea-ice condition on 24 March 2012, which is discussed in detail in Moore et al (19). Tundra site: 71.2751N, 156.6403W; NOAA Barrow Observatory: 71.3230N, 156.6114W; Barrow Arctic Research Center (BARC): 71.3250N, 156.6680W; Sea-ice site (frozen Chukchi Sea): 71.3227N, 156.7453W; and IceLander (frozen Beaufort Sea): 71.3550, 155.6680W. The wind direction range observed indicates influence from the Beaufort Sea, with no influence from the town of Utqiaġvik to the southeast.

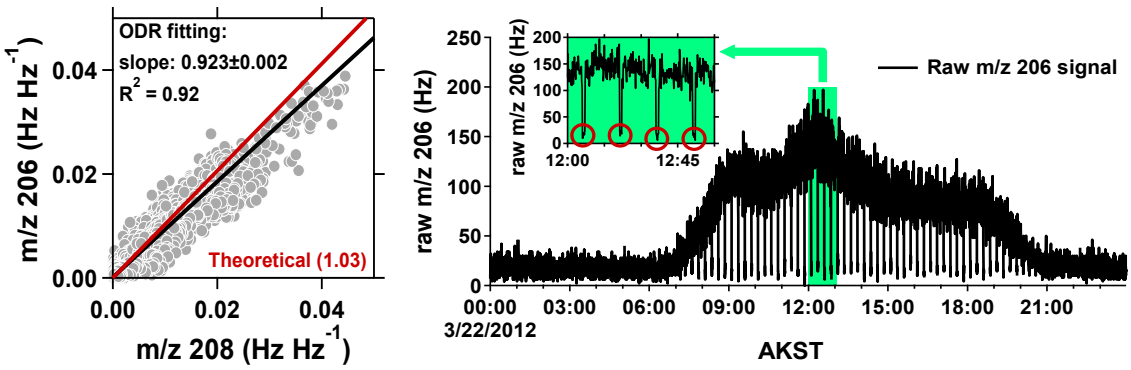

280

281 **Figure S2. (a) Background-subtracted 1-min averaged *m/z* 206 ($I^{79}Br^-$) vs *m/z* 208**
282 **($I^{81}Br^-$), each normalized by *m/z* 147 I($H_2{}^{18}O^-$), measured using CIMS during 14-28**
283 **March 2012 near Utqiaġvik, AK (tundra site). (b) The raw ambient *m/z* 206 signal is**
284 **shown for 22 March 2012, demonstrating that atomic bromine (IBr^-) was efficiently**
285 **removed by the glass wool scrubber during background periods (red circles).** The
286 theoretical slope based on bromine isotopes (1.03) is within 10% of that measured (0.92).

287

288 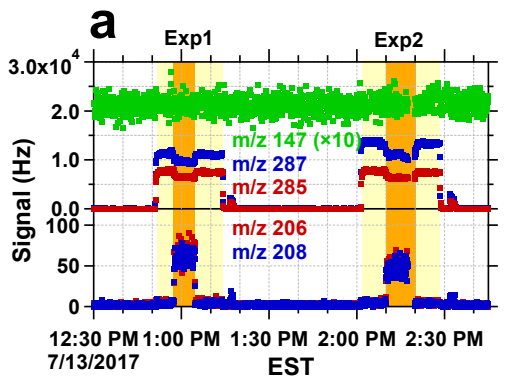

289 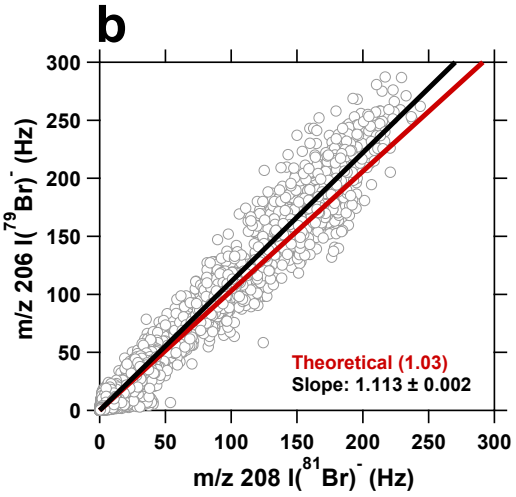

290 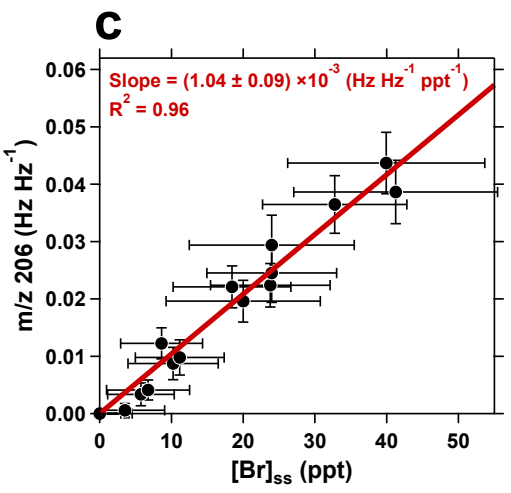

291 **Figure S3. (a) $I(H_2{}^{18}O)^-$ (*m/z* 147), $I^{79}Br^{79}Br^-$ (*m/z* 285), and $I^{79}Br^{81}Br^-$ (*m/z* 287) signals**
292 **measured during two laboratory flow tube experiments: (Exp1) 3.7 ppb Br_2 and 35**
293 **ppb CH_3CHO, and (Exp2) 3.9 ppb Br_2 and 48 ppb CH_3CHO, respectively.** Light
294 yellow shading indicates Br_2 injection in the dark, while orange shading shows periods

when the lights were on. *m/z* 285 ($I^{79}Br^{79}Br^-$) and *m/z* 287 ($I^{79}Br^{81}Br^-$) were both elevated with Br_2 injection under dark conditions. Upon irradiation, both *m/z* 285 and *m/z* 287 decreased while *m/z* 206 ($I^{79}Br^-$) and *m/z* 208 ($I^{81}Br^-$) increased, indicating atomic Br formation. **(b) Background-subtracted signals of *m/z* 206 $(I^{79}Br)^-$ vs. *m/z* 208 $(I^{81}Br)^-$ during all 15 Br atom calibration experiments.** Black and red lines denote ODR fitting of measured signals and the theoretical stable isotopic ratio of ^{79}Br / ^{81}Br (1.03), respectively. The measured slope (1.1) is within 7% of the theoretical value (1.03). **(c) Calibration curve for atomic Br ($I^{79}Br^-$, *m/z* 206), showing the normalized and background-subtracted signal versus the calculated steady-state Br atom mole ratio (ppt).** Each solid black circle is an average for a single calibration experiment (with Br_2 and / or CH_3CHO varied). Error bars represent the total measurement uncertainties, as described in the Methods.

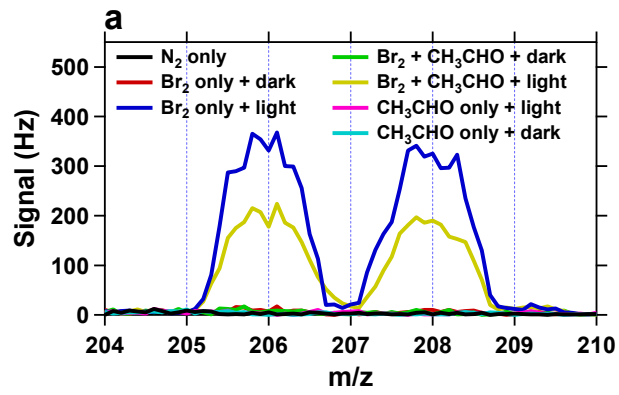

308

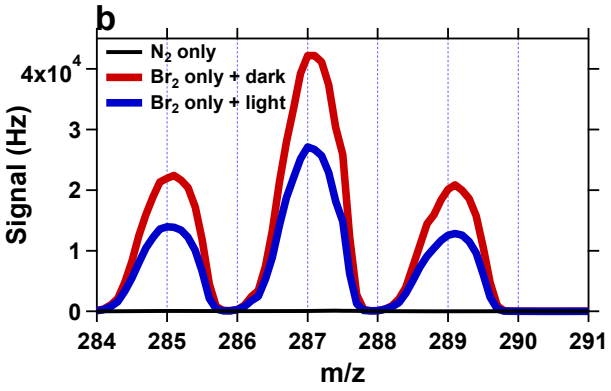

309

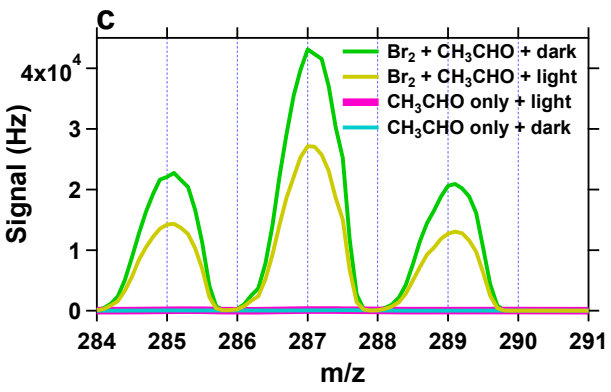

310

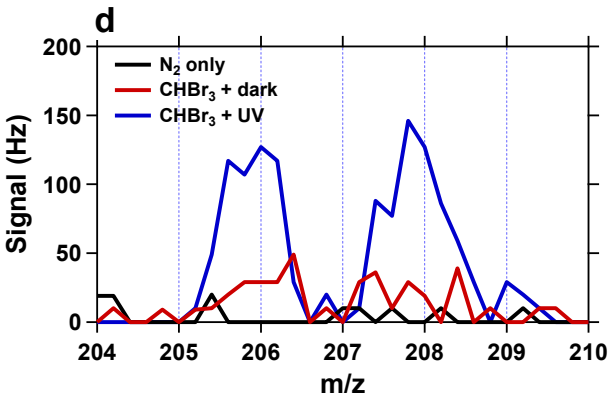

311

Figure S4. Mass scans of (a) *m/z* 204-210 for Br and (b, c) *m/z* 284-291 for Br_2 during the laboratory experiments when Br_2 and / or CH_3CHO were injected into the flow tube. The mass dwell times in (a), (b), and (c) were 1000 ms, and the step size was 0.1 amu. As shown in panel (a), with N_2 only, *m/z* 206 ($I^{79}Br^-$) and 208 ($I^{81}Br^-$) backgrounds (black) were below LODs until Br_2 was injected in the dark (red and green, without and with CH_3CHO). With Br_2 only and lights on, *m/z* 206 and 208 were both elevated (blue); slightly lower *m/z* 206 and 208 were observed when CH_3CHO was also injected (yellow). CH_3CHO alone (dark: cyan; light: pink; panels (b) and (c)) did not affect *m/z* 206 and 208 signals. As shown in panel (b), with N_2 only, *m/z* 285 ($I^{79}Br^{79}Br^-$), 287 ($I^{79}Br^{81}Br^-$), and 289 ($I^{81}Br^{81}Br^-$) backgrounds were all below LODs. When Br_2 was injected under dark conditions, *m/z* 285, 287, and 289 were all elevated (red in panel(b)); adding CH_3CHO (green, panel (c)) did not affect *m/z* 285, 287, and 289. When Br_2 was injected with the lights on, *m/z* 285, 287, and 289 were lower than with lights off (blue, panel (b)) due to photolysis; adding CH_3CHO (yellow, panel (c)) did not affect *m/z* 285, 287, and 289, as expected. **(d) Mass scans in the *m/z* 204-210 range during the laboratory tests with $CHBr_3$ injected into the flow tube.** The mass dwell time in (d) was 200 ms, and the step size was 0.2 amu. As shown in panel (d), with N_2 only, *m/z* 206 and 208 were both low (<19 Hz in this case). Elevated *m/z* 206 and 208 signals (<49 Hz) were observed with ~17 ppm $CHBr_3$ injected under dark conditions; upon irradiation, *m/z* 206 and 208 were elevated, consistent with the production of Br due to $CHBr_3$ photolysis.

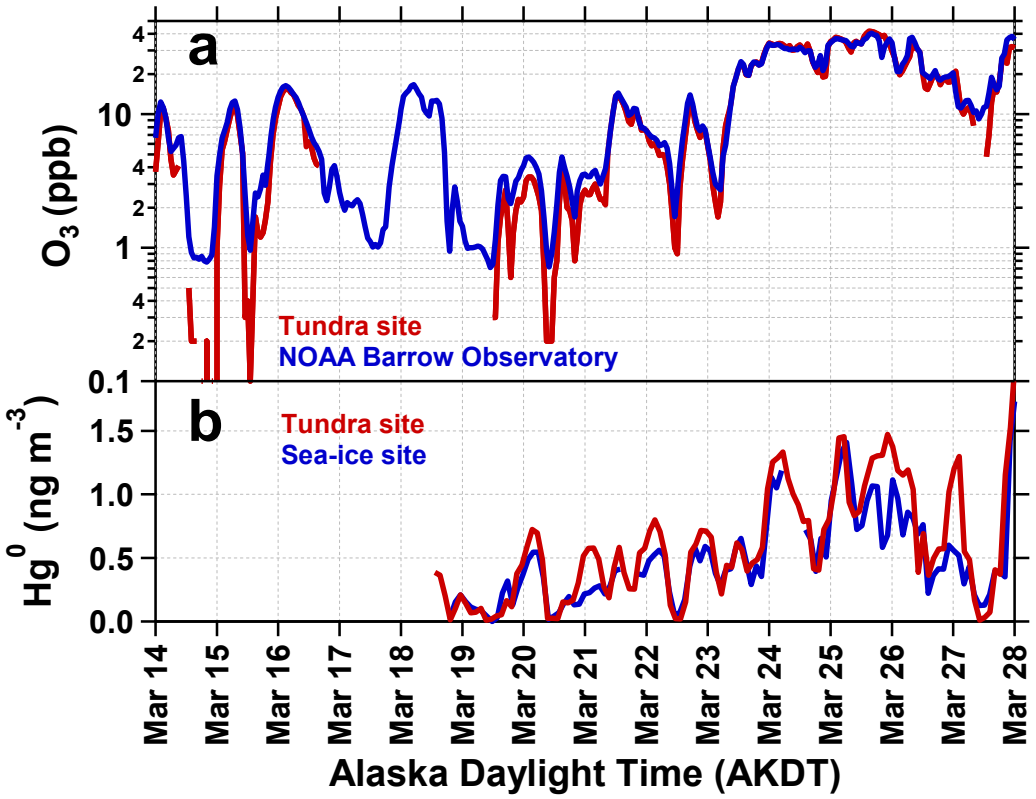

Figure S5. (a) O_3 measured at both the tundra site (2B Technologies model 205) and NOAA Barrow Observatory (Thermo Fisher model 49i); (b) Hg^0 measured at both the tundra site and sea-ice site. Differences in the O_3 measurements are due to differences in instrument limits of detection, as discussed in the Methods.

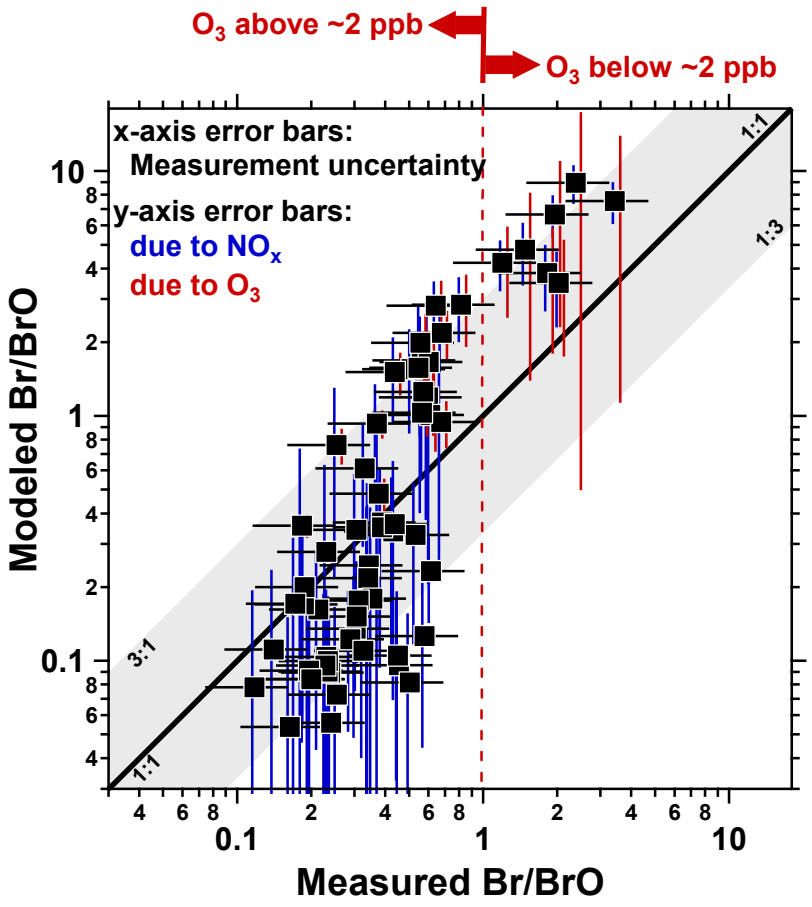

338

339 **Figure S6. Modeled Br/BrO ratio (with Br_2 constrained) vs measured.** As described in
340 Section S2, the model was constrained to measured Br_2, BrO, ClO, temperature, TUV-
341 calculated j-values. For the modeled Br/BrO ratios, the red error bars represent model
342 uncertainty due to O_3 measurement uncertainty (1 ppb), and blue error bars represent model
343 uncertainty due to the NO_x range (10-193 ppt).(13) Measured Br/BrO error bars are
344 propagated from CIMS measurement uncertainties of Br and BrO. Dark grey shading
345 indicates the kinetic uncertainties of bromine reactions at 250 K (total kinetic uncertainty:
346 82%; uncertainties of j-values are assumed to be 30%).(3)

347

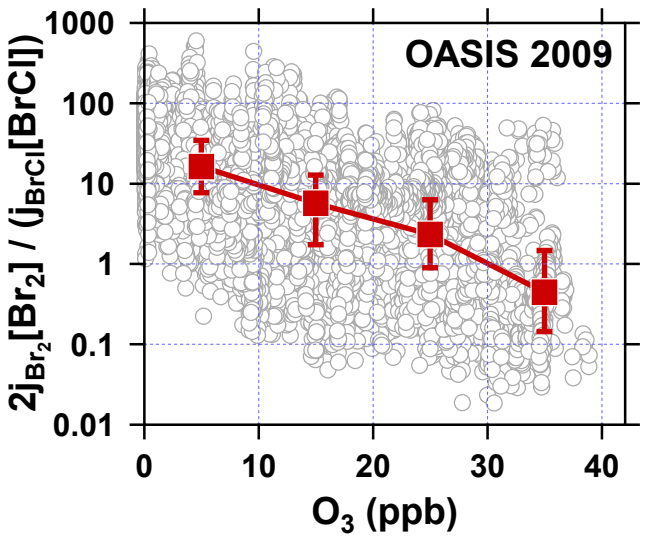

Figure S7. Calculated ratio between the Br production rate from the photolysis of measured Br_2 and the Br production rate from the photolysis of measured BrCl, as a function of measured O_3 during the OASIS field campaign in March 2009 near Utqiaġvik, AK. Grey circles are raw data, while red boxes are binned medians with 25% and 75% percentiles shown. Br_2 and BrCl were from CIMS measurements (9, 14), O_3 was measured using the chemiluminescence technique (13), and j-values were calculated using the Tropospheric Ultraviolet and Visible (TUV) radiation model based on in situ measurements of down-welling actinic flux conducted throughout the duration of the 2009 OASIS campaign (11) and a surface albedo of 0.9 (20).

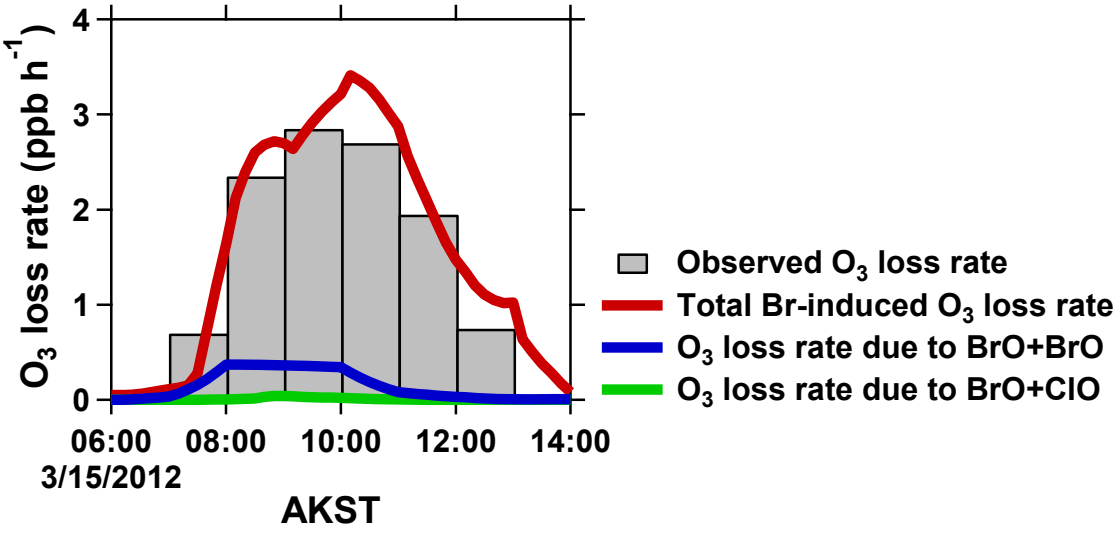

359

360 **Figure S8. Observed (gray) and calculated (red, blue, and green) O_3 loss rates for 15**
361 **March 2012 near Utqiaġvik, AK (tundra site).** The red line is the total bromine-induced
362 O_3 loss rate, as calculated using Equation S5. The blue and green lines are the O_3 loss rates
363 due to BrO+BrO and BrO+ClO, respectively, using Equation 2 in Thompson et al (15).

364

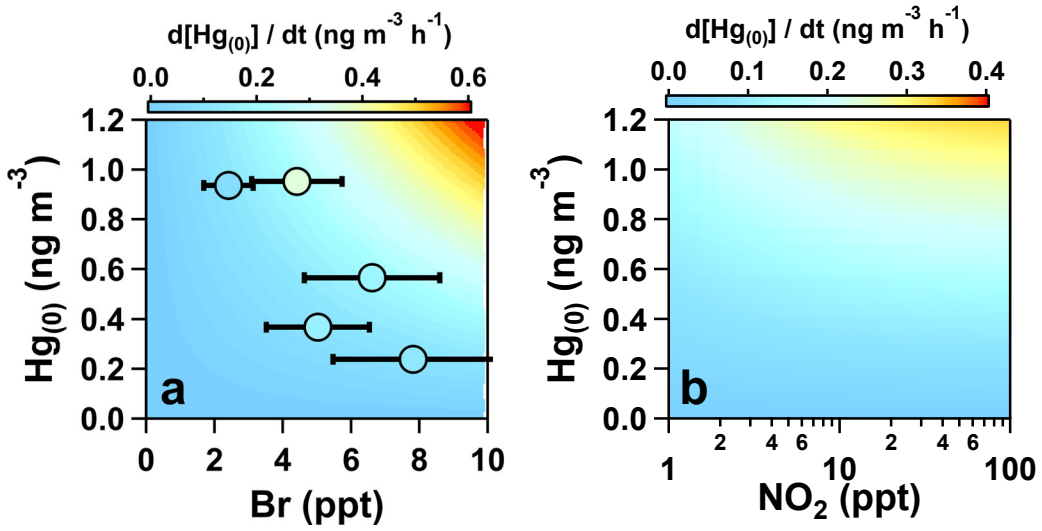

365

366 **Figure S9. Hg^0 loss rate as a function of (a) Br mole ratio and (b) NO_2 mole ratio,**
367 **color-coded by apparent Hg^0 loss rate.** Circles in panel (a) are the ambient observations
368 during BROMEX color-coded by the observed Hg^0 loss rate, and the background
369 corresponds to calculations (using R.S1-R.S6), assuming 250 K and 20 ppt NO_2. Panel (b)
370 assumes 250 K and 5 ppt Br.

371

372

373

Model inputs	Alert 2000 29 April – 6 May 2000		OASIS 2009 26-29 March 2009	
	Mean value	Ref.	Mean value	Ref.
j_{BrO} (s^{-1})	3.8×10^{-12} (max)	I	3.0×10^{-12} (max)	V
j_{Br2} (s^{-1})	4.3×10^{-12} (max)	I	4.4×10^{-12} (max)	V
NO (ppt)	4	II	21	V
O_3 (ppb)	1.7	III	0.3	V
BrO (ppt)	5	III	1.4	V
Br_2 (ppt)	Not available	-	2.5	V
HCHO (ppt)	166	IV	200	V
Temperature (K)	256	II	248	V
Modeled Br / BrO (ppt ppt^{-1})	**Alert 2000 29 April – 6 May 2000**		**OASIS 2009 26-29 March 2009**	
No Br_2	1.0		4.4	
With 1 ppt Br_2	1.5		10.3	
With observed Br_2	Not available		19.3	

374 **Table S1. Model inputs and calculated Br/BrO ratios for two ozone depletion events**
375 **observed in Alert, Canada (Alert 2000) and Utqiaġvik, Alaska (OASIS 2009).** The
376 Alert 2000 field campaign was conducted in Alert, Canada in April – May 2000; OASIS
377 2009 campaign was conducted near Utqiaġvik, Alaska in March – April 2009. Mean values
378 correspond to averages across the entire ODEs (except for j-values, for which maximum
379 values are provided). References: I. Calculated using NCAR TUV
380 (http://cprm.acom.ucar.edu/Models/TUV/Interactive_TUV/). II. Beine et al (21). III.
381 Honninger and Platt (22). IV. Grannas et al (23). V. Thompson et al (11).

382

References

1. Custard KD, Pratt KA, Wang S, Shepson PB (2016) Constraints on Arctic atmospheric chlorine production through measurements and simulations of Cl2 and ClO. *Environmental Science & Technology*. doi:10.1021/acs.est.6b03909.

2. Liao J, et al. (2011) A comparison of Arctic BrO measurements by chemical ionization mass spectrometry and long path-differential optical absorption spectroscopy. *Journal of Geophysical Research: Atmospheres (1984–2012)* 116(D1).

3. Burkholder JB, et al. (2015) Chemical Kinetics and Photochemical Data for Use in Atmospheric Studies, Evaluation No. 18. *JPL Publication 10-6, Jet Propulsion Laboratory, Pasadena, http://jpldataeval.jpl.nasa.gov* .

4. Ramacher B, Orlando JJ, Tyndall GS (2000) Temperature-dependent rate coefficient measurements for the reaction of bromine atoms with a series of aldehydes. *International Journal of Chemical Kinetics* 32(8):460–465.

5. Tang MJ, Cox RA, Kalberer M (2014) Compilation and evaluation of gas phase diffusion coefficients of reactive trace gases in the atmosphere: volume 1. Inorganic compounds. *Atmospheric Chemistry and Physics* 14(17):9233–9247.

6. Clyne MAA, Woon-Fat AR (1973) Recombination of ground state halogen atoms. Part 4.-Kinetics of recombination of bromine atoms. *Journal of the Chemical Society, Faraday Transactions 2: Molecular and Chemical Physics* 69(0):412–418.

7. Sjostedt SJ, et al. (2007) Observations of hydroxyl and the sum of peroxy radicals at Summit, Greenland during summer 2003. *Atmospheric Environment* 41(24):5122–5137.

8. Q-Lab Corporation (2011) Spectral power distribution for QUV with UVA-340 fluorescent lamps. Technical Bulletin LU-8052. Available at: Available at www.q-lab.com/products/%0Alamps-optical-filters/lamps-and-optical-filters.

9. Liao J, et al. (2012) Observations of inorganic bromine (HOBr, BrO, and Br2) speciation at Barrow, AK, in spring 2009. *Journal of Geophysical Research* 117(D00R16):doi:10.1029/2011JD016641.

10. Wang S, Pratt KA (2017) Molecular Halogens Above the Arctic Snowpack: Emissions, Diurnal Variations, and Recycling Mechanisms. *Journal of Geophysical Research: Atmospheres*:11,991–12,007.

11. Thompson CR, et al. (2015) Interactions of bromine, chlorine, and iodine photochemistry during ozone depletions in Barrow, Alaska. *Atmospheric Chemistry and Physics* 15(16):9651–9679.

12. Frenzel A, et al. (1998) Heterogeneous Interconversion Reactions of BrNO2, ClNO2, Br2, and Cl2. *The Journal of Physical Chemistry A* 102(8):1329–1337.

13. Villena G, et al. (2011) Nitrous acid (HONO) during polar spring in Barrow, Alaska: A net source of OH radicals? *Journal of Geophysical Research: Atmospheres* 116(D14):D00R07.

14. Liao J, et al. (2014) High levels of molecular chlorine in the Arctic atmosphere. *Nature Geosci* 7(2):91–94.

15. Thompson CR, et al. (2017) Bromine atom production and chain propagation during springtime Arctic ozone depletion events in Barrow, Alaska. *Atmospheric Chemistry and Physics* 17(5):3401–3421.

16. Simpson WR, et al. (2007) Halogens and their role in polar boundary-layer ozone depletion. *Atmospheric Chemistry and Physics* 7(16):4375–4418.

17. Horowitz HM, et al. (2017) A new mechanism for atmospheric mercury redox chemistry: implications for the global mercury budget. *Atmospheric Chemistry and Physics* 17(10):6353–6371.

18. Nghiem S V, et al. (2013) Studying Bromine, Ozone, and Mercury Chemistry in the Arctic. *Eos, Transactions American Geophysical Union* 94(33):289–291.

19. Moore CW, et al. (2014) Convective forcing of mercury and ozone in the Arctic boundary layer induced by leads in sea ice. *Nature* 506(7486):81–84.

20. Toyota K, McConnell JC, Staebler RM, Dastoor AP (2014) Air–snowpack exchange of bromine, ozone and mercury in the springtime Arctic simulated by the 1-D model PHANTAS Part 1: In-snow bromine activation and its impact on ozone. *Atmospheric Chemistry and Physics* 14(8):4101–4133.

21. Beine, J. H, Honrath, E. R, Florent D, Simpson, R. W, Fuentes, D. J (2002) NOx during background and ozone depletion periods at Alert: Fluxes above the snow surface. *Journal of Geophysical Research: Atmospheres* 107(D21):ACH 7-1-ACH 7-12.

22. Hönninger G, Platt U (2002) Observations of BrO and its vertical distribution during surface ozone depletion at Alert. *Atmospheric Environment* 36(15–16):2481–2489.

23. Grannas AM, et al. (2002) A study of photochemical and physical processes affecting carbonyl compounds in the Arctic atmospheric boundary layer. *Atmospheric Environment* 36(15–16):2733–2742.